Hindawi
Mathematical Problems in Engineering
Volume 2019, Article ID 1940784, 16 pages
https://doi.org/10.1155/2019/1940784

Research Article

Barrier Lyapunov Function-Based Adaptive Control of an Uncertain Hovercraft with Position and Velocity Constraints

Mingyu Fu, Taiqi Wang, and Chenglong Wang

College of Automation, Harbin Engineering University, Harbin 150001, China

Correspondence should be addressed to Taiqi Wang; wangtaiqi@hrbeu.edu.cn

Received 20 November 2018; Accepted 27 January 2019; Published 12 February 2019

Academic Editor: Sergey Dashkovskiy

This paper considers the problem of constrained path following control for an underactuated hovercraft subject to parametric uncertainties and external disturbances. A four-degree-of-freedom hovercraft model with unknown curve-fitted coefficients is first rewritten into a parameterized form. By introducing a barrier Lyapunov function into the line-of-sight guidance, the specific transient tracking performance in terms of position error is guaranteed. A novel constrained yaw rate controller is proposed to ensure time-varying yaw rate constraint satisfaction, in which the yaw rate barrier is required to vary with the speed of the hovercraft. Moreover, a command filter is incorporated into the control design to generate the desired virtual controls and its time derivatives. Theoretical analyses show that, under the proposed controller, the position tracking error constraints and the yaw rate constraint can be strictly guaranteed. Finally, numerical simulations illustrate the effectiveness and advantages of the proposed control scheme.

1. Introduction

As a high-performance amphibious marine craft, a hovercraft utilizes a flexible skirt system around its periphery such that the hull is totally supported by a pressurized air cushion. The hovercraft has attracted increasing attention in both military and civil fields because of its superior high speed and amphibious characteristics [1]. Due to its complex wave-making resistance and skirt drag caused by the cushion system, the dynamics of a hovercraft are very uncertain, nonlinear, and coupled [2]. Moreover, a hovercraft is underactuated because the actuators are equipped for surge and yaw motion only [3]. In addition, a hovercraft is essentially hovering over the water surface, which causes less water friction drag than conventional displacement ships. Therefore, a hovercraft can slip considerably and undergo great heeling during fast turning, requiring the yaw rate of a hovercraft to be regulated within specific safe ranges during maneuvering. These requirements make controller design of a hovercraft a challenging task.

Path following, which requires a hovercraft to follow a geometric path that is time independent, is one of the typical control scenarios for a marine surface vessel (MSV). In [4], a global path following controller was designed for MSVs based on a cascaded approach, and the stability was proved by using the linear time-varying theory. Reference [5] utilized a backstepping technique to develop a nonlinear path following controller for MSVs, in which the control design was based on feedback dominance instead of feedback linearization. Reference [6, 7] presented a model predictive control scheme with line-of-sight (LOS) guidance to improve the path following performance. Reference [8] proposed an adaptive path following controller to estimate the ocean currents, while a new integral LOS guidance law was obtained based on adaptive control. Neural network (NN) control is usually used to deal with the uncertain nonlinear system [9], which has also been widely introduced into path following control to cope with the uncertain dynamics of surface vessels. In [10, 11], the NN control approach together with the integral LOS guidance was proposed for underactuated surface vessels with parameter uncertainties. Reference [12] developed a saturated path following controller for surface vessels, and the uncertainties and disturbances were approximated by using NN.

One of the greatest challenges for hovercraft control is the inexact dynamics, which are due to the intricate interactions between the cushion system and the water surface; these interactions lead to an unclear hydrodynamic

structure and parametric uncertainties for control design. An exceedingly simplified hovercraft model was derived in [13–15], in which the hydrodynamic damping coefficients were assumed to be zero. The same hovercraft model was adopted in [16, 17]. However, because the hydrodynamic force and moment are not included in this model, the proposed model-based controllers might not achieve the desired control objective in practical applications. Furthermore, a curve-fitted hovercraft model was obtained in [1] by replacing the complex hydrodynamic and aerodynamic force and moment functions with curve-fitted approximations; by neglecting the heave and pitch motion, a four-degree-of-freedom (DOF) control-oriented hovercraft model was obtained for control design. However, the effects of parametric uncertainties and external disturbances were not considered in [1]. The uncertainties and disturbances always exist in a practical control system, and some works have investigated the feedback control schemes for different form uncertain nonlinear systems, such as triangular form systems [18, 19] and strict-feedback systems [20]. In addition, the adaptive control method is regarded as a powerful method to cope with such system uncertainties [21]. For example, [22] presented a backstepping-based adaptive control scheme to estimate the unknown parameters, and the tuning-function based approach was proposed to avoid the overparametrization in backstepping design. The adaptive backstepping technique has been widely applied in path following control of vessels [23–25]. To improve the tracking performance of a hovercraft under these system uncertainties, the above 4-DOF hovercraft dynamics [1] are rewritten into a parameterized form in this paper, and the adaptive control method is adopted to estimate the uncertain parameters and external disturbances.

LOS guidance, which has been widely explored for surface vessels due to its simplicity and small computational burden, is an effective guidance algorithm for path following control. In [26, 27], it was shown that the equilibrium point of the proportional LOS guidance law is uniformly and exponentially semi-globally stable. To compensate for the vehicle's constant sideslip due to environmental disturbances, an integral LOS (ILOS) approach was proposed in [28, 29] by adding an additive integral action into the conventional LOS guidance. In [10, 30], an adaptive LOS (ALOS)-based controller was developed with a parameter adaption law to eliminate the effects of system uncertainties. In [31], the authors discussed the drawbacks of the ILOS and ALOS. A modified extended state observer- (ESO-) based LOS guidance approach was proposed to identify the time-varying sideslip angle. Reference [32] presented a compound LOS guidance by combining the time delay control and ESO technique to estimate the time-varying ocean currents. Note that all the aforementioned LOS guidance algorithms only regulate the steady state of position tracking errors to be zero, while the transient tracking performance cannot be guaranteed. However, it is important to ensure the prescribed transient tracking performance of a hovercraft in practice. Moreover, the yaw rate of a hovercraft should be limited to below the stability boundary for safe navigation [33]. If the maximum yaw rate of a hovercraft exceeds the corresponding stability boundary for a period of time, the hovercraft will become unstable, especially at high speeds, which can even lead to a capsizing hazard. As shown in [33], the stability boundary of the yaw rate varies with the surge speed of a hovercraft. Thus, the yaw rate constraint should also be time varying because the desired speed command for a hovercraft can change in practice. To the author's knowledge, the problem of tracking error-constrained path following control for an uncertain hovercraft with a time-varying yaw rate constraint has rarely been considered.

To guarantee the state or output constraints of the system, some control methods have been included in model predictive control [34], nonovershooting control [35], and prescribed performance control [36]. However, in these methods, the state constraints remain difficult to guarantee in practical applications. More recently, a barrier Lyapunov function (BLF) has been proposed for nonlinear systems to ensure the state and output constraints [37, 38], which has been applied to strict-feedback systems with output constraints [39], pure-feedback systems [40], switched systems [41], and practical applications for hypersonic flight vehicles [42] or missile guidance [43]. In addition to the conventional logarithmic function form, a modified tan-type BLF was proposed in [44], which is a general method for systems with state constraints because it works even if the state constraints are removed. In [45], the authors utilized the tan-type BLF to design an error-constrained LOS path following controller for a 3-DOF conventional surface vessel. To break the static constraint limitations in the abovementioned works, a time-varying output constraint was handled in [46] by using a time-varying BLF, which allowed the output constraints to be both time varying and asymmetric. Moreover, to facilitate the backstepping design for the attitude subsystem of a hovercraft, a command filter was introduced to avoid the analytical computation of the virtual control laws [47].

Motivated by the above considerations, a BLF-based adaptive path following control scheme is developed for a 4-DOF underactuated hovercraft subject to parametric uncertainties and external disturbances. The main contributions of this paper can be summarized as follows:

(1) A novel position-constrained LOS guidance algorithm is proposed by introducing BLF into the classical LOS guidance design procedure. The proposed LOS guidance can guarantee the prescribed tracking performance in terms of position tracking errors.

(2) By virtue of the time-varying BLF, an attitude controller is proposed to ensure the yaw rate time-varying constraints of a hovercraft. The yaw rate of a hovercraft will not exceed the stability boundary, which has practical significance for the safe navigation of a hovercraft.

(3) A command filter is integrated into the control design to generate the amplitude-constrained virtual control laws, which avoid the analytic computation of the virtual control law derivative. In addition, a novel auxiliary system is developed to compensate for the filtering error.

The remainder of this paper is organized as follows. The problem formulation is introduced in Section 2. Section 3 is devoted to the LOS guidance, altitude subsystem, and velocity subsystem control design. Numerical simulation examples are presented in Section 4. Section 5 concludes the paper.

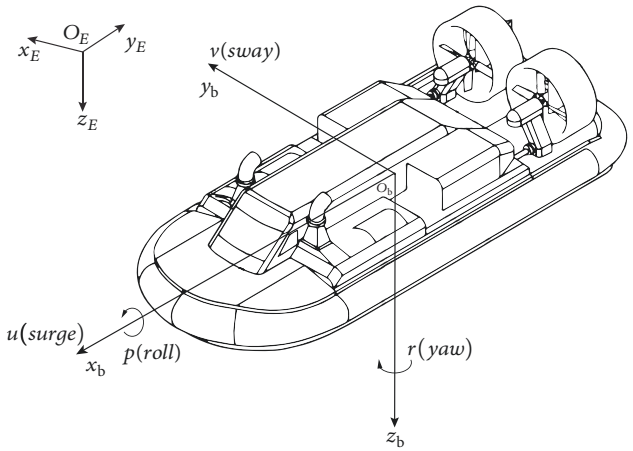

Figure 1: The hovercraft model in the body-fixed frame.

2. Problem Formulation and Preliminaries

2.1. Preliminaries

Notation. Throughout this paper, $(\cdot)^{\mathrm{T}}$ denotes the transpose of a matrix $(\cdot)$; $|\cdot|$ represents the absolute value of a scalar; $\|\cdot\|$ represents the Euclidean norm of a vector; $\hat{(\cdot)}$ denotes the estimate of $(\cdot)$; the estimation error is defined as $\tilde{(\cdot)} = (\cdot) - \hat{(\cdot)}$; and $\mathbb{R}^+$ denotes the set of nonnegative real numbers.

Lemma 1 (see [44]). *For any $\delta > 0$ and $\eta \in \mathbb{R}$, the following inequality always holds:*

$$0 \le |\eta| - \eta \tanh\left(\frac{\eta}{\delta}\right) \le 0.2785\delta \tag{1}$$

Lemma 2 (see [37]). *For any positive constant k_b, positive integer p, and $z \in \mathbb{R}$ satisfying $|z| < k_b$, there exists*

$$\log \frac{k_b^{2p}}{k_b^{2p} - z^{2p}} < \frac{z^{2p}}{k_b^{2p} - z^{2p}} \tag{2}$$

Definition 3 (see [39]). A barrier Lyapunov function is a scalar function $V(x)$ defined with respect to the system $\dot{x} = f(x)$ on an open region D containing the origin. It is continuous, is positive definite, has continuous first-order partial derivatives at every point of D, has the property $V(x) \longrightarrow \infty$ as x approaches the boundary of D, and satisfies $V(x) \le b$ $\forall t \ge 0$ along the solution of $\dot{x} = f(x)$ for $x(0) \in D$ and some positive constant b.

2.2. Dynamic Model of a Hovercraft.

The typical configuration of the hovercraft is shown in Figure 1, in which two sets of ducted air propellers are mounted at the stern and a pair of rudders is mounted behind the duct flaps to create turning moments.

For motion control of the hovercraft, we first define the earth-fixed frame $O_E x_E y_E z_E$ and the body-fixed frame $O_b x_b y_b z_b$. The origin of the body-fixed frame is located at the center of gravity (CG). By neglecting the pitch and heave motion and making some basic assumptions, the 4-DOF curve-fitted hovercraft dynamics are derived in [1] and are formulated as follows:

$$\begin{aligned}
\dot{u} &= vr + \frac{\left(F_{xa} + F_{xh} + F_{xn} + F_{xT}\right)}{m} \\
\dot{v} &= -ur + \frac{\left(F_{ya} + F_{yh} + F_{yc} + F_{yn}\right)}{m} \\
\dot{r} &= \frac{\left(M_{za} + M_{zh} + M_{zc} + M_{zn} + M_{z\delta}\right)}{I_z} \\
\dot{p} &= \frac{\left(M_{xa} + M_{xh} + M_{xc} + M_{xn} + M_{xG}\right)}{I_x}
\end{aligned} \tag{3}$$

where m is the mass of the hovercraft; I_x and I_z are the moments of inertia of the hovercraft about the x_b axis and z_b axis, respectively; u and v are the surge and sway linear velocities, respectively; and p and r represent the roll and yaw angular velocities, respectively. The right side of (3) consists of various forces and moments acting on the hovercraft, in which the suffix a represents the aerodynamic force, h denotes the hydrodynamic force, c denotes the cushion force, n denotes the air momentum force, T denotes the thrust, δ denotes the rudder moment, and G denotes the restoring moment during heeling of the hovercraft. The curve-fitted aerodynamic forces and moments in (3) are written as

$$\begin{aligned}
F_{xa} &= 0.5\rho_a V_a^2 S_{xa}\left(C_{xa0} + C_{xa}^{\delta_r}\delta_r + C_{xa}^{\beta}\beta + C_{xa}^{\dot{\beta}}\dot{\beta}\right) \\
F_{ya} &= 0.5\rho_a V_a^2 S_{ya}\left(C_{ya0} + C_{ya}^{\delta_r}\delta_r + C_{ya}^{\beta}\beta + C_{ya}^{\dot{\beta}}\dot{\beta}\right) \\
M_{za} &= 0.5\rho_a V_a^2 S_{za} l_a\left(C_{mza0} + C_{mza}^{\delta_r}\delta_r + C_{mza}^{\beta}\beta + C_{mza}^{\dot{\beta}}\dot{\beta}\right) \\
M_{xa} &= F_{ya} z_a
\end{aligned} \tag{4}$$

In addition, the curve-fitted hydrodynamic forces and moments in (3) are written as

$$\begin{aligned}
F_{xh} &= 0.5\rho_w U^2 S_h\left(C_{xh0} + C_{xh}^{\phi}\phi + C_{xh}^{\beta}\beta\right) \\
F_{yh} &= 0.5\rho_w U^2 S_h\left(C_{yh0} + C_{yh}^{\phi}\phi + C_{yh}^{\beta}\beta\right) \\
M_{zh} &= 0.5\rho_w U^2 S_h l_c\left(C_{mzh}^{\phi}\phi + C_{mzh}^{\beta}\beta\right) \\
M_{xh} &= F_{yh} z_g
\end{aligned} \tag{5}$$

where V_a denotes the relative wind speed. S_{xa}, S_{ya}, and S_{za} are the projection areas of the hovercraft along the three axes. The average length of the hovercraft is denoted by l_a, the vertical distance from the center of the lateral area is denoted by z_a, the velocity of the hovercraft is denoted by $U = \sqrt{u^2 + v^2}$, the lateral area of the skirts in contact with the water surface is denoted by S_h, the cushion length is denoted by l_c, and the height of CG is defined as z_g. δ_r, ϕ, and β represent the rudder angle, heeling angle, and sideslip angle of the hovercraft, respectively. $C_*^{\#}$ represents the curve-fitted coefficient. The expressions of other component forces and moments can be found in [1] (Chapter 6).

In this paper, we assume that S_{xa}, S_{ya}, S_{za}, S_h, and $C_*^{\#}$ in (4) and (5) are unknown constants. Thus, (4) and (5) can be parameterized into the following form:

$$\begin{aligned}
\frac{F_{xa}}{m} &= \vartheta_{u,1}^{\mathrm{T}}\varphi_{u,1} \\
\frac{F_{ya}}{m} &= \vartheta_{v,1}^{\mathrm{T}}\varphi_{v,1} \\
\frac{M_{za}}{I_z} &= \vartheta_{r,1}^{\mathrm{T}}\varphi_{r,1} \\
\frac{M_{xa}}{I_x} &= \vartheta_{p,1}^{\mathrm{T}}\varphi_{p,1}, \\
\frac{F_{xh}}{m} &= \vartheta_{u,2}^{\mathrm{T}}\varphi_{u,2} \\
\frac{F_{yh}}{m} &= \vartheta_{v,2}^{\mathrm{T}}\varphi_{v,2} \\
\frac{M_{zh}}{I_z} &= \vartheta_{r,2}^{\mathrm{T}}\varphi_{r,2} \\
\frac{M_{xh}}{I_x} &= \vartheta_{p,2}^{\mathrm{T}}\varphi_{p,2}
\end{aligned} \tag{6}$$

By substituting (6) and other component forces and moments into (3), a 4-DOF parameterized hovercraft model can be given as

$$\begin{aligned}
\dot{u} &= vr + f_u + \vartheta_{u,1}^{\mathrm{T}}\varphi_{u,1} + \vartheta_{u,2}^{\mathrm{T}}\varphi_{u,2} + \tau_u + d_u \\
\dot{v} &= -ur + f_v + \vartheta_{v,1}^{\mathrm{T}}\varphi_{v,1} + \vartheta_{v,2}^{\mathrm{T}}\varphi_{v,2} + d_v \\
\dot{r} &= f_r + \vartheta_{r,1}^{\mathrm{T}}\varphi_{r,1} + \vartheta_{r,2}^{\mathrm{T}}\varphi_{r,2} + \tau_r + d_r \\
\dot{p} &= f_p + \vartheta_{p,1}^{\mathrm{T}}\varphi_{p,1} + \vartheta_{p,2}^{\mathrm{T}}\varphi_{p,2} + d_p
\end{aligned} \tag{7}$$

where the control inputs in (7) are $\tau_u = F_{xT}/m$ and $\tau_r = M_{z\delta}/I_z$. The dynamics f_u, f_v, f_p, and f_r are the integration of other known component forces and moments in (3), which are defined as $f_u = F_{xn}/m$, $f_v = (F_{yc} + F_{yn})/m$, $f_r = (M_{zc} + M_{zn})/I_z$, and $f_p = (M_{xc} + M_{xn} + M_{xG})/I_x$. In addition, d_u, d_v, d_r, and d_p in (7) denote the bounded disturbances, including the unmodeled dynamics and external disturbances induced by wind and waves. See Appendix B for the detailed expressions of the parameters in (7).

The desired parameterized path is defined by $X_p = (x_p(\omega), y_p(\omega))$, where $\omega \in \mathbb{R}$ denotes the path variable. A path-fixed reference frame is defined with its origin at X_p. The path-tangential angle is calculated by

$$\gamma_p(\omega) = \operatorname{atan2}\left(y_p'(\omega), x_p'(\omega)\right) \tag{8}$$

where $x_p'(\omega) = \partial x_p/\partial\omega$ and $y_p'(\omega) = \partial y_p/\partial\omega$. For a hovercraft located at $X = (x, y)$, the geometry of LOS guidance is illustrated in Figure 2.

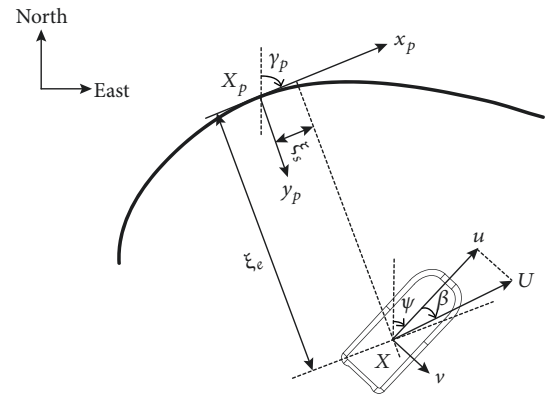

Figure 2: The LOS guidance geometry.

The along-track error $\xi_s(t)$ and the cross-track error $\xi_e(t)$ in the path-fixed frame are written as

$$\begin{bmatrix}\xi_s \\ \xi_e\end{bmatrix} = \begin{bmatrix}\cos\gamma_p & -\sin\gamma_p \\ \sin\gamma_p & \cos\gamma_p\end{bmatrix}^{\mathrm{T}}\begin{bmatrix}x - x_p \\ y - y_p\end{bmatrix} \tag{9}$$

According to the kinematic equations of surface vessels given in [48], the 4-DOF kinematics of the hovercraft is expressed as

$$\begin{bmatrix}\dot{x} \\ \dot{y} \\ \dot{\psi} \\ \dot{\phi}\end{bmatrix} = \begin{bmatrix}\cos\psi & -\sin\psi\cos\phi & 0 & 0 \\ \sin\psi & \cos\psi\cos\phi & 0 & 0 \\ 0 & 0 & \cos\phi & 0 \\ 0 & 0 & 0 & 1\end{bmatrix}\begin{bmatrix}u \\ v \\ r \\ p\end{bmatrix} \tag{10}$$

where x and y are the coordinates of the hovercraft's CG in the earth-fixed frame. ψ is the heading angle of the hovercraft, and ϕ is the heeling angle of the hovercraft.

The time derivative of the tracking errors in (9) is written as

$$\begin{aligned}
\begin{bmatrix}\dot{\xi}_s \\ \dot{\xi}_e\end{bmatrix} = \dot{\gamma}_p &\begin{bmatrix}\underbrace{-\sin\gamma_p\left(x - x_p\right) + \cos\gamma_p\left(y - y_p\right)}_{\xi_e} \\ \underbrace{-\cos\gamma_p\left(x - x_p\right) - \sin\gamma_p\left(y - y_p\right)}_{-\xi_s}\end{bmatrix} \\
&+ \begin{bmatrix}\cos\gamma_p\left(\dot{x} - \dot{x}_p\right) + \sin\gamma_p\left(\dot{y} - \dot{y}_p\right) \\ -\sin\gamma_p\left(\dot{x} - \dot{x}_p\right) + \cos\gamma_p\left(\dot{y} - \dot{y}_p\right)\end{bmatrix}
\end{aligned} \tag{11}$$

Substituting (8) and (10) into (11) yields

$$\begin{aligned}
\begin{bmatrix}\dot{\xi}_s \\ \dot{\xi}_e\end{bmatrix} = &\begin{bmatrix}u\cos\left(\psi - \gamma_p\right) - \overline{v}\sin\left(\psi - \gamma_p\right) - \dot{\omega}\sqrt{x_p'^2 + y_p'^2} \\ u\sin\left(\psi - \gamma_p\right) + \overline{v}\cos\left(\psi - \gamma_p\right)\end{bmatrix} \\
&+ \begin{bmatrix}\dot{\gamma}_p\xi_e \\ -\dot{\gamma}_p\xi_s\end{bmatrix}
\end{aligned} \tag{12}$$

Setting $\beta = \operatorname{atan2}(\overline{v}, u)$, (12) can finally be written as

$$\begin{bmatrix}\dot{\xi}_s \\ \dot{\xi}_e\end{bmatrix} = \begin{bmatrix}\overline{U}\cos\left(\psi - \gamma_p + \beta\right) - \dot{\omega}\sqrt{x_p'^2 + y_p'^2} + \dot{\gamma}_p\xi_e \\ \overline{U}\sin\left(\psi - \gamma_p + \beta\right) - \dot{\gamma}_p\xi_s\end{bmatrix} \tag{13}$$

where $\overline{v} = v\cos\phi$ is the projection of the lateral velocity onto the horizontal plane. $\overline{U} = \sqrt{u^2 + \overline{v}^2}$ is the hovercraft speed. If

the roll motion is not considered, we obtain $\cos\phi = 1$. The obtained equation (13) is similar to the previous results [8, 31] for 3-DOF surface vessels.

Suppose that k_s, k_e, and k_{u_e} are positive constant constraints and $k_r(t)$ is the symmetric time-varying yaw rate constraint, where the time derivatives of k_s, k_e, k_{u_e}, and $k_r(t)$ are bounded. The control objective of this study is to design a constrained path following controller for a hovercraft in the presence of parametric uncertainties and external disturbances that can guarantee the prescribed tracking performance: $|\xi_s| < k_s$ and $|\xi_e| < k_e$. The yaw rate satisfies the constraint $|r(t)| < k_r(t)$, and the surge velocity satisfies the constraint $|u_e| < k_{u_e}$ for all $t > 0$, where $u_e = u - u_d$.

Remark 4. In the previous path following literature [8, 10, 29, 31], the proposed LOS guidance algorithms only regulate the steady-state tracking errors to be zero or within the neighborhood of zero, while the transient tracking performances are not considered. Reference [45] also proposed a LOS guidance to limit the position tracking errors. However, only the output constraints of the vessel were guaranteed; the yaw rate and velocity constraints were not guaranteed. In this paper, both the state and the output constraints of vessel system can be strictly guaranteed by the proposed control scheme. In addition, the yaw rate of a hovercraft is of particular concern to sailors during maneuver. Because the hovercraft usually hovers over the water with a high forward velocity, a large yaw rate or an excessive rudder angle can easily influence the navigation safety of a hovercraft as compared to a conventional displacement ship. Reference [33] shows that the stability boundary of the yaw rate varies with the surge speed of the hovercraft, which leads to the conversion of our design task into a time-varying state constrained problem.

To facilitate the control design, we make the following assumptions.

Assumption 5. The disturbances $d_u(t)$, $d_v(t)$, $d_r(t)$, and $d_p(t)$ are bounded. There exist unknown positive constants D_u, D_v, D_r, and D_p such that $|d_u| \le D_u$, $|d_v| \le D_v$, $|d_r| \le D_r$. and $|d_p| \le D_p$ hold for all $t \ge 0$.

Assumption 6. The initial tracking errors $\xi_s(0)$, $\xi_e(0)$, and $u_e(0)$ satisfy the prescribed constraints $|\xi_s(0)| < k_s$, $|\xi_e(0)| < k_e$, and $|u_e(0)| < k_{u_e}$, and the yaw rate tracking error satisfies $|r_e(0)| < k_{r_e}(0)$.

Assumption 7. For any $k_s > 0$ and $k_e > 0$, the first and second time derivatives of the desired path (x_p, y_p) are both bounded.

Assumption 8. Due to underactuated configuration of the hovercraft, a constraint on sway dynamics without control input is required that the sway velocity of the hovercraft is passive bounded.

3. Control System Design

3.1. Position-Constrained LOS Guidance. In this subsection, the barrier Lyapunov function will be introduced into the LOS guidance to guarantee the position constraints. The Lyapunov function is defined as follows:

$$V_1 = \frac{1}{2}\log\frac{k_s^2}{k_s^2 - \xi_s^2} + \frac{1}{2}\log\frac{k_e^2}{k_e^2 - \xi_e^2} \tag{14}$$

The time derivative of V_1 is calculated as

$$\dot{V}_1 = \vartheta_s\dot{\xi}_s + \vartheta_e\dot{\xi}_e \tag{15}$$

where $\vartheta_s = \xi_s/(k_s^2 - \xi_s^2)$ and $\vartheta_e = \xi_e/(k_e^2 - \xi_e^2)$.

Substituting (13) into (15), we obtain

$$\begin{aligned}\dot{V}_1 &= \vartheta_s\left(\overline{U}\cos\left(\psi - \gamma_p + \beta\right) - \dot{\omega}\sqrt{x_p'^2 + y_p'^2} + \dot{\gamma}_p\xi_e\right)\\ &\quad + \vartheta_e\left(\overline{U}\sin\left(\psi - \gamma_p + \beta\right) - \dot{\gamma}_p\xi_s\right)\\ &= \vartheta_s\left(\overline{U}\cos\left(\psi - \gamma_p + \beta\right) - \dot{\omega}\sqrt{x_p'^2 + y_p'^2}\right)\\ &\quad + \vartheta_s\dot{\gamma}_p\xi_e\left(1 - \frac{k_s^2 - \xi_s^2}{k_e^2 - \xi_e^2}\right) + \vartheta_e\overline{U}\sin\left(\psi - \gamma_p + \beta\right)\end{aligned} \tag{16}$$

Taking the time derivative of γ_p yields

$$\dot{\gamma}_p = \dot{\omega}\frac{y_p''x_p' - x_p''y_p'}{x_p'^2 + y_p'^2} \tag{17}$$

Invoking (17) in (16), we have

$$\begin{aligned}\dot{V}_1 &= \vartheta_s\left(\overline{U}\cos\left(\psi - \gamma_p + \beta\right) - \dot{\omega}\sigma\right)\\ &\quad + \vartheta_e\overline{U}\sin\left(\psi - \gamma_p + \beta\right)\end{aligned} \tag{18}$$

with

$$\sigma = \sqrt{x_p'^2 + y_p'^2} - \xi_e\frac{y_p''x_p' - x_p''y_p'}{x_p'^2 + y_p'^2}\left(1 - \frac{k_s^2 - \xi_s^2}{k_e^2 - \xi_e^2}\right) \tag{19}$$

Defining the tracking error as

$$\psi_e = \psi - \psi_d \tag{20}$$

and substituting (20) into (18) yield

$$\begin{aligned}\dot{V}_1 &= \vartheta_s\left(\overline{U}\cos\left(\psi - \gamma_p + \beta\right) - \dot{\omega}\sigma\right)\\ &\quad + \vartheta_e\left(\left(u_d\sin\left(\psi_d - \gamma_p\right) + \overline{v}\cos\left(\psi_d - \gamma_p\right)\right)\cos\psi_e\right.\\ &\quad + u_e\sin\left(\psi - \gamma_p\right)\\ &\quad \left. + \left(u_d\cos\left(\psi_d - \gamma_p\right) - \overline{v}\sin\left(\psi_d - \gamma_p\right)\right)\sin\psi_e\right)\\ &= \vartheta_s\left(\overline{U}\cos\left(\psi - \gamma_p + \beta\right) - \dot{\omega}\sigma\right)\\ &\quad + \vartheta_e\left(\overline{U}_d\sin\left(\psi_d - \gamma_p + \overline{\beta}_d\right)\cos\psi_e + u_e\sin\left(\psi - \gamma_p\right)\right.\\ &\quad \left. + \overline{U}_d\cos\left(\psi_d - \gamma_p + \overline{\beta}_d\right)\sin\psi_e\right)\end{aligned} \tag{21}$$

with $\overline{U}_d = \sqrt{u_d^2 + \overline{v}^2}$ and $\overline{\beta}_d = \text{atan2}(\overline{v}, u_d)$.

From (21), we can obtain the update law for ω:

$$\dot{\omega} = \frac{\overline{U}\cos\left(\psi - \gamma_p + \beta\right) + k_1\xi_s}{\sigma} \tag{22}$$

Note that σ is the denominator of (22); to avoid $\sigma = 0$, we can take $\sigma = \sigma_0\,\mathrm{sgn}(\sigma)$ when $|\sigma| < \sigma_0$, where σ_0 is a small positive constant.

The desired heading angle of the hovercraft is chosen to be

$$\psi_d = \gamma_p - \overline{\beta}_d + \mathrm{atan2}\left(-\xi_e, k_2\right) \tag{23}$$

where $k_1, k_2 > 0$ are positive design constants and k_2 is the look-ahead distance.

By invoking (22) and (23), (21) becomes

$$\begin{aligned}\dot{V}_1 &= \frac{-k_1\xi_s^2}{k_s^2 - \xi_s^2} + \vartheta_e\left(\frac{-\cos\psi_e\overline{U}_d\xi_e + \sin\psi_e\overline{U}_d k_2}{\sqrt{k_2^2 + \xi_e^2}}\right.\\ &\quad\left. + u_e\sin\left(\psi - \gamma_p\right)\right)\\ &= -\frac{k_1\xi_s^2}{k_s^2 - \xi_s^2} - \frac{\overline{U}_d}{\sqrt{k_2^2 + \xi_e^2}}\frac{\xi_e^2}{k_e^2 - \xi_e^2} + \vartheta_e\psi_e\chi + \vartheta_e u_e\\ &\quad\cdot\sin\left(\psi - \gamma_p\right) \le -\varsigma_1 V_1 + \vartheta_e\psi_e\chi + \vartheta_e u_e\sin\left(\psi - \gamma_p\right)\end{aligned} \tag{24}$$

where

$$\chi = -\frac{\overline{U}_d\xi_e}{\sqrt{k_2^2 + \xi_e^2}}\frac{\left(\cos\psi_e - 1\right)}{\psi_e} + \frac{k_2\overline{U}_d}{\sqrt{k_2^2 + \xi_e^2}}\frac{\sin\psi_e}{\psi_e} \tag{25}$$

with $\varsigma_1 = \min\{k_1, \overline{U}_d/\sqrt{k_2^2 + \xi_e^2}\}$.

Remark 9. In (25), we have $|\xi_e|/\sqrt{k_2^2 + \xi_e^2} \le 1$ and $k_2/\sqrt{k_2^2 + \xi_e^2} \le 1$. By using L'Hopital's rule, we obtain $\lim_{\psi_e \to 0}((\cos\psi_e - 1)/\psi_e) = 0$ and $\lim_{\psi_e \to 0}(\sin\psi_e/\psi_e) = 1$. Thus, singularity will not occur in (25).

3.2. Attitude Control. In this subsection, the attitude kinematic controller for the hovercraft will be designed to stabilize the yaw angle tracking error ψ_e. Subsequently, the yaw rate controller will be developed via BLF-based adaptive control, while the time-varying constraint on the yaw rate, $|r| < k_r(t)$, will be strictly guaranteed.

Suppose that the virtual yaw rate α_r satisfies

$$\left|\alpha_r\right| < k_{\alpha_r}(t) < k_r(t) \tag{26}$$

where $k_{\alpha_r}(t) : \mathbb{R}^+ \longrightarrow \mathbb{R}^+$ and $k_r(t) : \mathbb{R}^+ \longrightarrow \mathbb{R}^+$. The yaw rate tracking error is defined as $r_e = r - \alpha_r$. If a yaw rate controller exists that can ensure the inequality

$$\left|r_e\right| < k_{r_e}(t) \le k_r(t) - k_{\alpha_r}(t) \tag{27}$$

where $k_{r_e}(t) : \mathbb{R}^+ \longrightarrow \mathbb{R}^+$ and then the time-varying constraint $k_r(t)$ on yaw rate $r(t)$ can be guaranteed.

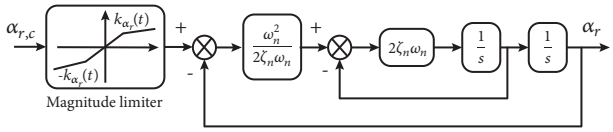

Figure 3: Configuration of the command filter.

Remark 10. If the designed yaw rate controller can make $|r_e| < k_{r_e}(t)$, then we have $|r - \alpha_r| < k_r(t) - k_{\alpha_r}(t)$ and $|r| - |\alpha_r| < k_r(t) - k_{\alpha_r}(t)$. Using (26), we obtain $|r| < k_r(t) - (k_{\alpha_r}(t) - \alpha_r) < k_r(t)$.

However, one problem is how to ensure the inequality $|\alpha_r| < k_{\alpha_r}(t)$ in (26) because there is no effective mechanism to guarantee it. Motivated by [49], the command filter is employed to constrain the magnitude of the virtual yaw rate by the time-varying constraint $k_{\alpha_r}(t)$. The command filter is shown in Figure 3.

Here, the nominal virtual yaw rate $\alpha_{r,c}$ is filtered to provide the magnitude and bandwidth limited virtual yaw rate α_r and its derivative $\dot{\alpha}_r$. In addition, an auxiliary system will be designed to compensate for the estimation error $\Delta\alpha_r = \alpha_r - \alpha_{r,c}$.

Step 1 (kinematics controller). Choose the following candidate Lyapunov function V_2:

$$V_2 = \frac{1}{2}\psi_e^2 \tag{28}$$

Taking the time derivative of (28), we obtain

$$\dot{V}_2 = \psi_e\left(r_e\cos\phi + \Delta\alpha_r\cos\phi + \alpha_{r,c}\cos\phi - \dot{\psi}_d\right) \tag{29}$$

To avoid the complex derivative computations of ψ_d included in the nominal virtual control law $\alpha_{r,c}$, a second-order tracking-differentiator [50, 51] will be used for the estimation of $\dot{\psi}_d$, which is described as

$$\begin{aligned}\dot{\nu}_1 &= \nu_2\\ \dot{\nu}_2 &= -R^2\left[a_1\left(\nu_1 - \psi_d\right) + a_2\frac{\nu_2}{R}\right]\end{aligned} \tag{30}$$

where R, a_1, and a_2 are positive design constants; ψ_d is the input signal of (30); ν_1 and ν_2 denote the respective estimations of ψ_d and $\dot{\psi}_d$. Let $\nu_2 = \dot{\psi}_{d,c}$ and define the estimation error as

$$\varepsilon = \dot{\psi}_{d,c} - \dot{\psi}_d \tag{31}$$

According to Theorem 2 presented in [50], we have $\lim_{R \to +\infty}\varepsilon = 0$, which means that ε can be sufficiently small by choosing a large R. Hence, it can be concluded that there exists arbitrarily small positive constant ε_M such that $|\varepsilon| \le \varepsilon_M$.

As such, the nominal virtual control law $\alpha_{r,c}$ for (29) is given by

$$\alpha_{r,c} = \frac{-k_3\psi_e + \dot{\psi}_{d,c} - \vartheta_e\chi + c_1\zeta_r - \left(c_1^2/2\right)\psi_e}{\cos\phi} \tag{32}$$

where $k_3 > 1/2$ and $c_1 > 0$ denote the design constants. $\phi \neq \pm\pi/2$. ζ_r is the state of the auxiliary system and compensates for the constraint effect $\Delta\alpha_r$. The auxiliary system is designed as

$$\dot{\zeta}_r = \begin{cases} -k_4\zeta_r - f_1\zeta_r + \gamma_1\Delta\alpha_r\cos\phi, & |\zeta_r| > \rho_1 \\ 0, & |\zeta_r| \le \rho_1 \end{cases} \tag{33}$$

where $k_4 > 1$ and $\gamma_1 > 0$. ρ_1 is a small positive design constant that satisfies the performance requirement. f_1 is given by

$$f_1 = \frac{\left|\psi_e\Delta\alpha_r\cos\phi\right| + (1/2)\,\gamma_1^2\left(\Delta\alpha_r\cos\phi\right)^2}{\left|\zeta_r\right|^2} \tag{34}$$

Remark 11. Note that, in (33), ζ_r will exponentially converge onto the small set $|\zeta_r| \le \rho_1$ if $\Delta\alpha_r = 0$. If the state ζ_r in (33) satisfies $|\zeta_r| > \rho_1$, then saturation effects occur again and the initial value of the auxiliary system should be properly reset to ensure that ζ_r can respond to the case $\Delta\alpha_r \neq 0$.

Consider the candidate Lyapunov function

$$V_3 = V_2 + \frac{1}{2}\zeta_r^2 \tag{35}$$

Invoking (32) and (33), the time derivative of V_3 is given by

$$\begin{aligned} \dot{V}_3 &= \psi_e\left(\left(r_e + \Delta\alpha_r\right)\cos\phi - k_3\psi_e + \left(\dot{\psi}_{d,c} - \dot{\psi}_d\right) - \vartheta_e\chi\right. \\ &\quad \left. + c_1\zeta_r - \frac{c_1^2}{2}\psi_e\right) + \zeta_r\left(-k_4\zeta_r - f_1\zeta_r + \gamma_1\Delta\alpha_r\cos\phi\right) \\ &= \psi_e r_e\cos\phi + \psi_e\Delta\alpha_r\cos\phi + \psi_e\varepsilon - \vartheta_e\psi_e\chi + c_1\psi_e\zeta_r \\ &\quad - k_3\psi_e^2 - k_4\zeta_r^2 - \left|\psi_e\Delta\alpha_r\cos\phi\right| - \frac{1}{2}\gamma_1^2\left(\Delta\alpha_r\cos\phi\right)^2 \\ &\quad - \frac{c_1^2}{2}\psi_e^2 + \gamma_1\zeta_r\Delta\alpha_r\cos\phi \end{aligned} \tag{36}$$

Note that, in (36),

$$\begin{aligned} \psi_e\varepsilon &\le \frac{1}{2}\psi_e^2 + \frac{1}{2}\varepsilon_M^2, \\ c_1\psi_e\zeta_r &\le \frac{1}{2}c_1^2\psi_e^2 + \frac{1}{2}\zeta_r^2, \\ \gamma_1\zeta_r\Delta\alpha_r\cos\phi &\le \frac{1}{2}\gamma_1^2\left(\Delta\alpha_r\cos\phi\right)^2 + \frac{1}{2}\zeta_r^2. \end{aligned} \tag{37}$$

Then, we have

$$\begin{aligned} \dot{V}_3 &\le -\left(k_3 - \frac{1}{2}\right)\psi_e^2 - \left(k_4 - 1\right)\zeta_r^2 - \vartheta_e\psi_e\chi + \psi_e r_e\cos\phi \\ &\quad + \frac{1}{2}\varepsilon_M^2 \le -\varsigma_2 V_3 - \vartheta_e\psi_e\chi + \psi_e r_e\cos\phi + \frac{1}{2}\varepsilon_M^2 \end{aligned} \tag{38}$$

where $\varsigma_2 = \min\{k_3 - 1/2, k_4 - 1\}$.

Step 2 (dynamics controller). Consider the following time-varying symmetric BLF:

$$V_4 = \frac{1}{2}\log\frac{k_{r_e}^2(t)}{k_{r_e}^2(t) - r_e^2} \tag{39}$$

where $k_{r_e}(t) : \mathbb{R}^+ \longrightarrow \mathbb{R}^+$. Recalling *Remark 10*, the constrained yaw rate controller will be proposed to guarantee the constraint $|r_e| < k_{r_e}(t)$. Define the new variable as $\xi_r = r_e/k_{r_e}$; (39) can be rewritten as

$$V_4 = \frac{1}{2}\log\frac{1}{1 - \xi_r^2} \tag{40}$$

It can be seen that V_4 is positive definite and continuously differentiable in the set $|\xi_r| < 1$. The time derivative of V_4 is calculated as

$$\dot{V}_4 = \vartheta_r\left(\dot{r}_e - r_e\frac{\dot{k}_{r_e}}{k_{r_e}}\right) \tag{41}$$

with $\vartheta_r = \xi_r/k_{r_e}(1 - \xi_r^2)$.

Substituting the third equation of (7) into (41), we have

$$\dot{V}_4 = \vartheta_r\left(f_r + \vartheta_{r,1}^{\mathrm{T}}\varphi_{r,1} + \vartheta_{r,2}^{\mathrm{T}}\varphi_{r,2} + \tau_r + d_r - \dot{\alpha}_r - r_e\frac{\dot{k}_{r_e}}{k_{r_e}}\right) \tag{42}$$

The yaw rate control law for (42) becomes

$$\begin{aligned} \tau_r &= -f_r - \widehat{\vartheta}_{r,1}^{\mathrm{T}}\varphi_{r,1} - \widehat{\vartheta}_{r,2}^{\mathrm{T}}\varphi_{r,2} + \dot{\alpha}_r - k_5 r_e - \overline{k}_5 r_e \\ &\quad - \left(k_{r_e}^2 - r_e^2\right)\psi_e\cos\phi - \widehat{D}_r\tanh\left(\frac{\vartheta_r}{\sigma_r}\right) \end{aligned} \tag{43}$$

where $\overline{k}_5 = \sqrt{(\dot{k}_{r_e}/k_{r_e})^2 + \varpi}$, with $\varpi > 0$ a small constant. $k_5 > 0$ and $\sigma_r > 0$ are design constants. $\dot{\alpha}_r$ is directly obtained from the output of the command filter. $\widehat{\vartheta}_{r,1}^{\mathrm{T}}$, $\widehat{\vartheta}_{r,2}^{\mathrm{T}}$, and $\widehat{D}_r$ are adaptive estimations of $\vartheta_{r,1}^{\mathrm{T}}$, $\vartheta_{r,2}^{\mathrm{T}}$, and D_r, respectively.

The adaptation laws for $\widehat{\vartheta}_{r,1}$, $\widehat{\vartheta}_{r,2}$, and $\widehat{D}_r$ are designed as follows:

$$\begin{aligned} \dot{\widehat{\vartheta}}_{r,1} &= \vartheta_r\varphi_{r,1} - k_{\vartheta,1}\widehat{\vartheta}_{r,1} \\ \dot{\widehat{\vartheta}}_{r,2} &= \vartheta_r\varphi_{r,2} - k_{\vartheta,2}\widehat{\vartheta}_{r,2} \\ \dot{\widehat{D}}_r &= \vartheta_r\tanh\left(\frac{\vartheta_r}{\sigma_r}\right) - k_6\widehat{D}_r \end{aligned} \tag{44}$$

where $k_{\vartheta,1}$, $k_{\vartheta,2}$, and k_6 are positive design constants.

Next, we construct the candidate Lyapunov function as follows:

$$V_5 = V_4 + \frac{1}{2}\widetilde{\vartheta}_{r,1}^T\widetilde{\vartheta}_{r,1} + \frac{1}{2}\widetilde{\vartheta}_{r,2}^T\widetilde{\vartheta}_{r,2} + \frac{1}{2}\widetilde{D}_r^2 \tag{45}$$

Taking the time derivative of (45) and using (42) and (44), we obtain

$$\begin{aligned} \dot{V}_5 &= \dot{V}_4 - \widetilde{\vartheta}_{r,1}^T\dot{\widehat{\vartheta}}_{r,1} - \widetilde{\vartheta}_{r,2}^T\dot{\widehat{\vartheta}}_{r,2} - \widetilde{D}_r\dot{\widehat{D}}_r \\ &\le -k_5\frac{\xi_r^2}{1 - \xi_r^2} - \left(\overline{k}_5 + \frac{\dot{k}_{r_e}}{k_{r_e}}\right)r_e\vartheta_r + k_{\vartheta,1}\widetilde{\vartheta}_{r,1}^{\mathrm{T}}\widehat{\vartheta}_{r,1} \\ &\quad + k_{\vartheta,2}\widetilde{\vartheta}_{r,2}^{\mathrm{T}}\widehat{\vartheta}_{r,2} + \vartheta_r\left(d_r - D_r\tanh\left(\frac{\vartheta_r}{\sigma_r}\right)\right) + k_6\widetilde{D}_r\widehat{D}_r \\ &\quad - \psi_e r_e\cos\phi \end{aligned} \tag{46}$$

Note that

$$\bar{k}_5 + \frac{\dot{k}_{r_e}}{k_{r_e}} \geq \left|\bar{k}_5\right| - \left|\frac{\dot{k}_{r_e}}{k_{r_e}}\right| > 0 \tag{47}$$

$$\widetilde{\vartheta}_{r,1}^{\mathrm{T}}\widehat{\vartheta}_{r,1} \leq \frac{\left\|\vartheta_{r,1}\right\|^2 - \left\|\widetilde{\vartheta}_{r,1}\right\|^2}{2},$$

$$\widetilde{\vartheta}_{r,2}^{\mathrm{T}}\widehat{\vartheta}_{r,2} \leq \frac{\left\|\vartheta_{r,2}\right\|^2 - \left\|\widetilde{\vartheta}_{r,2}\right\|^2}{2}, \tag{48}$$

$$\widetilde{D}_r\widehat{D}_r \leq \frac{D_r^2 - \widetilde{D}_r^2}{2}$$

and

$$\vartheta_r\left(d_r - D_r\tanh\left(\frac{\vartheta_r}{\sigma_r}\right)\right) \leq 0.2785\sigma_r D_r \tag{49}$$

Substituting the inequalities (47)-(49) and (2) into (46), in the set, $|\xi_r| < 1$ we can obtain that

$$\begin{aligned}\dot{V}_5 &\leq -2k_5V_4 - \left(\bar{k}_5 + \frac{\dot{k}_{r_e}}{k_{r_e}}\right)\frac{\xi_r^2}{1-\xi_r^2} - \frac{k_{\vartheta,1}}{2}\left\|\widetilde{\vartheta}_{r,1}\right\|^2 \\ &\quad - \frac{k_{\vartheta,2}}{2}\left\|\widetilde{\vartheta}_{r,2}\right\|^2 - \frac{k_6}{2}\widetilde{D}_r^2 + \mu_r - \psi_e r_e\cos\phi \\ &\leq -2k_5V_4 - \frac{k_{\vartheta,1}}{2}\left\|\widetilde{\vartheta}_{r,1}\right\|^2 - \frac{k_{\vartheta,2}}{2}\left\|\widetilde{\vartheta}_{r,2}\right\|^2 - \frac{k_6}{2}\widetilde{D}_r^2 + \mu_r \\ &\quad - \psi_e r_e\cos\phi \leq -\varsigma_3V_5 + \mu_r - \psi_e r_e\cos\phi\end{aligned} \tag{50}$$

where $\varsigma_3 = \min\{2k_5, k_{\vartheta,1}, k_{\vartheta,2}, k_6\}$, with μ_r a positive constant defined as

$$\mu_r = \frac{k_{\vartheta,1}}{2}\left\|\vartheta_{r,1}\right\|^2 + \frac{k_{\vartheta,2}}{2}\left\|\vartheta_{r,2}\right\|^2 + \frac{k_6}{2}D_r^2 + 0.2785\sigma_r D_r. \tag{51}$$

3.3. Velocity Tracking Control. In this subsection, the designed control force τ_u should enforce the following constraint on the velocity: $\lim_{t\to\infty}u(t) \longrightarrow u_d(t)$. In addition, the constraint $|u_e| < k_{u_e}$ should also be strictly guaranteed. Using the first equation in (7), the time derivative of u_e is calculated as

$$\dot{u}_e = vr + f_u + \vartheta_{u,1}^{\mathrm{T}}\varphi_{u,1} + \vartheta_{u,2}^{\mathrm{T}}\varphi_{u,2} + \tau_u + d_u - \dot{u}_d \tag{52}$$

Choosing the barrier Lyapunov function

$$V_6 = \frac{1}{2}\log\frac{k_{u_e}^2}{k_{u_e}^2 - u_e^2} \tag{53}$$

and differentiating (53) yield

$$\dot{V}_6 = \vartheta_u\dot{u}_e \tag{54}$$

where $\vartheta_u = u_e/(k_{u_e}^2 - u_e^2)$.

We design the surge velocity tracking controller for τ_u as follows:

$$\begin{aligned}\tau_u &= -vr - \widehat{\vartheta}_{u,1}^{\mathrm{T}}\varphi_{u,1} - \widehat{\vartheta}_{u,2}^{\mathrm{T}}\varphi_{u,2} - \widehat{D}_u\tanh\left(\frac{\vartheta_u}{\sigma_u}\right) - f_u \\ &\quad - k_7u_e + \dot{u}_d - \vartheta_e\left(k_{u_e}^2 - u_e^2\right)\sin\left(\psi - \gamma_p\right)\end{aligned} \tag{55}$$

where $k_7 > 0$ and $\sigma_u > 0$ are design constants.

The adaptation laws for $\widehat{\vartheta}_{u,1}$, $\widehat{\vartheta}_{u,2}$, and $\widehat{D}_u$ are given as

$$\begin{aligned}\dot{\widehat{\vartheta}}_{u,1} &= \vartheta_u\varphi_{u,1} - k_{\vartheta,3}\widehat{\vartheta}_{u,1} \\ \dot{\widehat{\vartheta}}_{u,2} &= \vartheta_u\varphi_{u,2} - k_{\vartheta,4}\widehat{\vartheta}_{u,2} \\ \dot{\widehat{D}}_u &= \vartheta_u\tanh\left(\frac{\vartheta_u}{\sigma_u}\right) - k_8\widehat{D}_u\end{aligned} \tag{56}$$

where $k_{\vartheta,3}$, $k_{\vartheta,4}$, and k_8 are positive design constants.

Construct the Lyapunov function V_7 as

$$V_7 = V_6 + \frac{1}{2}\widetilde{\vartheta}_{u,1}^{\mathrm{T}}\widetilde{\vartheta}_{u,1} + \frac{1}{2}\widetilde{\vartheta}_{u,2}^{\mathrm{T}}\widetilde{\vartheta}_{u,2} + \frac{1}{2}\widetilde{D}_u^2 \tag{57}$$

Taking the time derivative of (57) and invoking (54)-(56), we obtain

$$\begin{aligned}\dot{V}_7 &= \dot{V}_6 - \widetilde{\vartheta}_{u,1}^{\mathrm{T}}\dot{\widehat{\vartheta}}_{u,1} - \widetilde{\vartheta}_{u,2}^{\mathrm{T}}\dot{\widehat{\vartheta}}_{u,2} - \widetilde{D}_u\dot{\widehat{D}}_u \\ &\leq -k_7\frac{u_e^2}{k_{u_e}^2 - u_e^2} + k_{\vartheta,3}\widetilde{\vartheta}_{u,1}^{\mathrm{T}}\widehat{\vartheta}_{u,1} + k_{\vartheta,4}\widetilde{\vartheta}_{u,2}^{\mathrm{T}}\widehat{\vartheta}_{u,2} + k_8\widetilde{D}_u\widehat{D}_u \\ &\quad + \vartheta_u\left(d_u - D_u\tanh\left(\frac{\vartheta_u}{\sigma_u}\right)\right) - \vartheta_e u_e\sin\left(\psi - \gamma_p\right)\end{aligned} \tag{58}$$

Note also that $\widetilde{\vartheta}_{u,1}^{\mathrm{T}}\widehat{\vartheta}_{u,1} \leq (\|\vartheta_{u,1}\|^2 - \|\widetilde{\vartheta}_{u,1}\|^2)/2$, $\widetilde{\vartheta}_{u,2}^{T}\widehat{\vartheta}_{u,2} \leq (\|\vartheta_{u,2}\|^2 - \|\widetilde{\vartheta}_{u,2}\|^2)/2$, and $\widetilde{D}_u\widehat{D}_u \leq (D_u^2 - \widetilde{D}_u^2)/2$.

We then have

$$\begin{aligned}\dot{V}_7 &\leq -2k_7V_6 - \frac{k_{\vartheta,3}}{2}\left\|\widetilde{\vartheta}_{u,1}\right\|^2 - \frac{k_{\vartheta,4}}{2}\left\|\widetilde{\vartheta}_{u,2}\right\|^2 - \frac{k_8}{2}\widetilde{D}_u^2 + \mu_u \\ &\quad - \vartheta_e u_e\sin\left(\psi - \gamma_p\right) \\ &\leq -\varsigma_4V_7 + \mu_u - \vartheta_e u_e\sin\left(\psi - \gamma_p\right)\end{aligned} \tag{59}$$

where $\varsigma_4 = \min\{2k_7, k_{\vartheta,3}, k_{\vartheta,4}, k_8\}$ and μ_u is a positive constant defined as

$$\mu_u = \frac{k_{\vartheta,3}}{2}\left\|\vartheta_{u,1}\right\|^2 + \frac{k_{\vartheta,4}}{2}\left\|\vartheta_{u,2}\right\|^2 + \frac{k_8}{2}D_u^2 + 0.2578\sigma_u D_u. \tag{60}$$

Remark 12. In (55), the desired surge speed $u_d(t)$ is required to be continuously differentiable. In previous works [10, 11, 45], the desired surge speed u_d was chosen as a constant for all $t > 0$. However, in practice, the desired surge speed of a hovercraft is often directly switched to another value, which will lead to the nonexistence of $\dot{u}_d(t)$. Thus, to ensure that the desired surge speed is differentiable when u_d changes from u_{d1} to u_{d2} between any time interval t_a and t_b, we give a speed smoother as follows:

$$u_d = u_{d1} + h\left(t, t_a, t_b, \gamma_t\right)\left(u_{d2} - u_{d1}\right) \tag{61}$$

The scalar function $h(t, t_a, t_b, \gamma_t)$ is defined as

$$h\left(t, t_a, t_b, \gamma_t\right) = \frac{f\left(\tau\right)}{f\left(\tau\right) + \gamma_t f\left(1-\tau\right)} \tag{62}$$

where $\tau = (t - t_a)/(t_b - \gamma_t)$. $f(\tau) = 0$ if $\tau \leq 0$, and $f(\tau) = e^{-1/\tau}$ if $\tau > 0$, with $t_a < t_b$ and γ_t a positive constant. The speed smoother is shown in Figure 4.

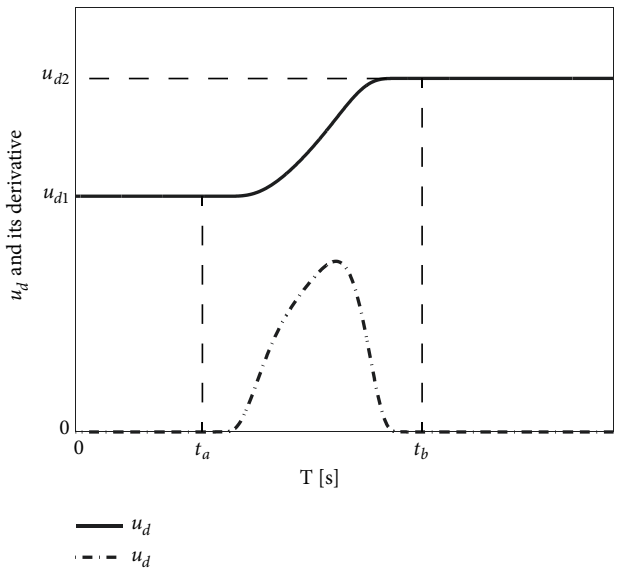

Figure 4: The desired surge speed and its derivative.

3.4. Stability Analysis

Theorem 13. *Consider the parameterized hovercraft models (7) and (10) in the presence of parametric uncertainties and external disturbances and assume that Assumptions 5–8 are satisfied. If the update law for the path variable ω is chosen as (22), the desired heading angle of the hovercraft is calculated by (23), the auxiliary system is designed as (33), the adaptation laws for unknown parameters and external disturbances are given by (44) and (56), and the controllers are obtained from (43) and (55); then the following properties hold:*

(i) All the error signals in the closed-loop system are uniformly ultimately bounded (UUB).

(ii) The static constraints on position and surge velocity tracking errors and the time-varying constraints on the yaw rate are never violated, i.e., $|\xi_s| < k_s$, $|\xi_e| < k_e$, $|u_e| < k_{u_e}$ and $|r(t)| < k_r(t)$ hold for all $t > 0$.

Proof. (i) Construct the following candidate Lyapunov function:

$$V = V_1 + V_3 + V_5 + V_7 \tag{63}$$

By virtue of (24), (38), (50), and (59), the time derivative of V is given by

$$\begin{aligned}\dot{V} &\le -\varsigma_1 V_1 - \varsigma_2 V_3 - \varsigma_3 V_5 - \varsigma_4 V_7 + \vartheta_e \psi_e \chi + \mu_r \\ &\quad + \vartheta_e u_e \sin\left(\psi - \gamma_p\right) - \vartheta_e \psi_e \chi + \psi_e r_e \cos\phi \\ &\quad - \psi_e r_e \cos\phi - \vartheta_e u_e \sin\left(\psi - \gamma_p\right) + \frac{1}{2}\varepsilon_M^2 + \mu_u \\ &\le -\varsigma_1 V_1 - \varsigma_2 V_3 - \varsigma_3 V_5 - \varsigma_4 V_7 + \mu_u + \mu_r + \frac{1}{2}\varepsilon_M^2 \\ &\le -\varsigma_V V + \mu_V\end{aligned} \tag{64}$$

where $\varsigma_V = \min\{\varsigma_1, \varsigma_2, \varsigma_3, \varsigma_4\}$ and $\mu_V = \mu_u + \mu_r + (1/2)\varepsilon_M^2$.

If the initial conditions satisfy *Assumption 6*, then the constructed Lyapunov function V satisfies the inequality

$$V(t) \le \Gamma(t) = \left(V(0) - \frac{\mu_V}{\varsigma_V}\right)\exp\left(-\varsigma_V t\right) + \frac{\mu_V}{\varsigma_V} \tag{65}$$

From (65), we know that $\lim_{t\to\infty} V(t) \le \lim_{t\to\infty}\Gamma(t) = \mu_V/\varsigma_V$. Therefore, all the error signals in the closed-loop system are uniformly ultimately bounded. Noting the expressions of μ_V and ς_V, the ultimate bounds can be made arbitrarily small by adjusting the design parameters.

(ii) $\forall t > 0$, the BLF (14), (40), and (53) satisfy the following inequalities:

$$\begin{aligned}\frac{1}{2}\log\frac{k_i^2}{k_i^2 - \xi_i^2} &\le V(t) \le \Gamma(t) \\ \frac{1}{2}\log\frac{k_{u_e}^2}{k_{u_e}^2 - u_e^2} &\le V(t) \le \Gamma(t) \\ \frac{1}{2}\log\frac{1}{1 - \xi_r^2} &\le V(t) \le \Gamma(t)\end{aligned} \tag{66}$$

where $i = s, e$.

Then, from (66), we obtain

$$\begin{aligned}|\xi_s| &\le k_s\sqrt{1 - \exp\left(-2\Gamma(t)\right)} < k_s \\ |\xi_e| &\le k_e\sqrt{1 - \exp\left(-2\Gamma(t)\right)} < k_e \\ |u_e| &\le k_{u_e}\sqrt{1 - \exp\left(-2\Gamma(t)\right)} < k_{u_e} \\ |\xi_r| &\le \sqrt{1 - \exp\left(-2\Gamma(t)\right)} < 1\end{aligned} \tag{67}$$

In (67), from $|\xi_r| < 1$, $\forall t > 0$, we know that $|r_e(t)| < k_{r_e}(t), \forall t > 0$. Recalling *Remark 10*, we conclude that $|r(t)| < k_r(t)$. Therefore, all the prescribed constraints of the hovercraft system can be guaranteed for $\forall t > 0$. This completes the proof. □

4. Simulation

In this section, numerical simulations will be implemented to demonstrate the effectiveness and safety of the proposed control scheme for hovercraft navigation and to compare our scheme with the results presented in [11, 45]. A general curvilinear path simulation scenario is considered. In simulations, the uncertainty parameters in (7), including S_{xa}, S_{ya}, S_{za}, S_h, and $C_*^\#$, have 20% maximum relative uncertainties according to their nominal values; i.e., their real values are chosen according to

$$\begin{aligned}S_* &= S_{*\text{nominal}} + \lambda S_{*\text{nominal}}, \\ C_*^\# &= C_{*\text{nominal}}^\# + \lambda C_{*\text{nominal}}^\#,\end{aligned} \tag{68}$$

where λ is randomly selected from $[-0.2, 0.2]$. The nominal parameters of the hovercraft are shown in Appendix A,

Table 1: Nominal values of the hovercraft in the simulation.

Parameter	Nominal Value	SI-Unit	Parameter	Nominal Value	SI-Unit
C_{xa0}	-0.345	-	C_{yh0}	-0.00011	-
$C_{xa}^{\delta_r}$	-0.00516	1/rad	C_{yh}^{ϕ}	-0.0012	1/rad
C_{xa}^{β}	-0.2504	1/rad	$C_{yh}^{\dot{\beta}}$	0.04582	1/rad
$C_{xa}^{\dot{\beta}}$	-0.0001	s/rad	C_{mza0}	-0.000356	-
C_{xh0}	-0.1049	-	$C_{mza}^{\delta_r}$	-0.001534	1/rad
C_{xh}^{ϕ}	0.00014	1/rad	C_{mza}^{β}	-0.05412	1/rad
C_{xh}^{β}	0.191	1/rad	$C_{mza}^{\dot{\beta}}$	-0.00021	s/rad
C_{ya0}	-0.001	-	C_{mzh}^{ϕ}	0	1/rad
$C_{ya}^{\delta_r}$	0.002614	1/rad	C_{mzh}^{β}	0	1/rad
C_{ya}^{β}	0.1645	1/rad	m	40000	kg
$C_{ya}^{\dot{\beta}}$	0.00042	s/rad	I_x	247810	kgm^2
S_{xa}	45.27	m^2	I_z	1746347	kgm^2
S_{ya}	93	m^2	S_{za}	268	m^2
S_h	21	m^2			

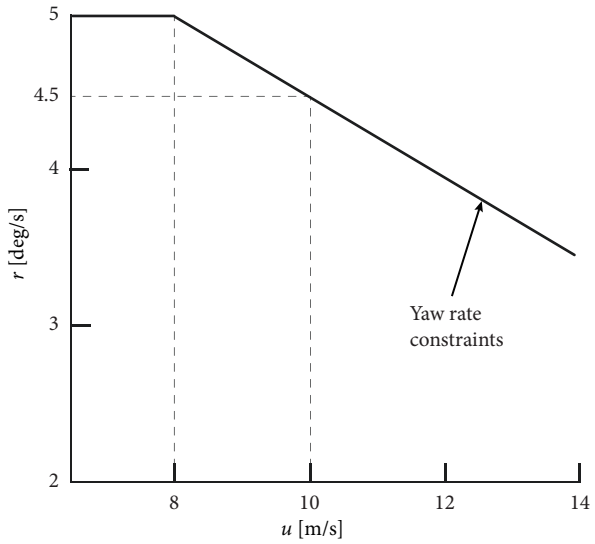

Figure 5: The yaw rate constraints on the hovercraft.

Table 1. For numerical simulations, the time-varying bounded disturbances in (7) are generated by using the first-order Gauss-Markov process [52]:

$$\begin{aligned} \dot{d}_u + a_1 d_u &= \omega_1 \\ \dot{d}_v + a_2 d_v &= \omega_2 \\ \dot{d}_r + a_3 d_r &= \omega_3 \\ \dot{d}_p + a_4 d_p &= \omega_4 \end{aligned} \tag{69}$$

where ω_i $(i = 1, 2, 3, 4)$ are zero-mean Gaussian white noise processes and $a_i \geq 0$ $(i = 1, 2, 3, 4)$ are constants.

To demonstrate that the control objective can be achieved by the proposed controller, we first set the constant constraints on position and surge velocity to be $k_s = 30$ m, $k_e = 30$ m, and $k_{u_e} = 1$ m/s. The time-varying yaw rate constraint in our simulations is shown in Figure 5, which is similar to the yaw rate constraint in [33]. We can see that the yaw rate constraint of the hovercraft decreases with increasing surge speed. To adapt to practical applications, it is determined that the yaw rate should be further restricted to guarantee the navigation safety of a hovercraft with a higher speed. The yaw rate constraint $k_r(t)$ can be written as $k_r(t) = -0.25u(t) + 7$, with $u(t) \geq 8$ m/s. The maximum yaw rate tracking error is limited by $|r_e| \leq 1$ deg/s. Thus, the time-varying magnitude of the limiter in Figure 3 is set as $k_{\alpha_r}(t) = -0.25u(t) + 6$, with $u(t) \geq 8$ m/s, and the yaw rate tracking error constraints should satisfy the conditions: $k_{r_e}(t) \leq k_r(t) - k_{\alpha_r}(t) = 1$ deg/s. The control parameters are listed in Table 2.

In addition to our proposed controller, we simulate two different controllers for comparison, which are assigned as follows.

Case 1. This comparative controller is derived from [11] by using traditional adaptive LOS guidance. The yaw rate constraint is not considered.

Case 2. This comparative controller is designed by using the strategy in [45], which can only guarantee the position constraints. However, the yaw rate constraint is not considered.

Case 3. This controller in this case is our proposed control scheme.

The desired path for a curvilinear path following simulation is given as $X_p = [\omega, 2000 \sin(\omega/550)]^{\mathrm{T}}$ m. The initial positions of the hovercraft are chosen as $(x(0), y(0), \psi(0)) = (29\,\mathrm{m}, 29\,\mathrm{m}, 0\,\mathrm{rad})$, the initial velocities are $(u(0), v(0)) = (7.5\,\mathrm{m/s}, 0\,\mathrm{m/s})$, and $r(0) = 0.0087$ rad/s. The initial states of the hovercraft satisfy Assumption 6, and according to (61), the desired surge speed $u_d(t)$ varies from 8 m/s to 10 m/s between $t_a = 406$ s and $t_b = 410$ s. For comparison purposes, the desired surge speed in Cases 1 and 2 is directly switched from 8 m/s to 10 m/s at $t_s = 408$ s. To analyse the control performances under these three controllers, simulation results are given as follows.

The path following results in Figure 6 demonstrate that the proposed controller has improved performance in terms

Table 2: Control parameters in hovercraft simulations.

Parameter	Value	Parameter	Value
k_1	2	σ_u	0.1
k_2	80	σ_r	0.1
k_3	1	$k_{\vartheta,1}$	5
c_1	0.1	$k_{\vartheta,2}$	3
k_4	1.5	$k_{\vartheta,3}$	1.5
k_5	0.01	$k_{\vartheta,4}$	4
$\overline{k}_5$	3	k_7	1
k_6	20	k_8	0.2

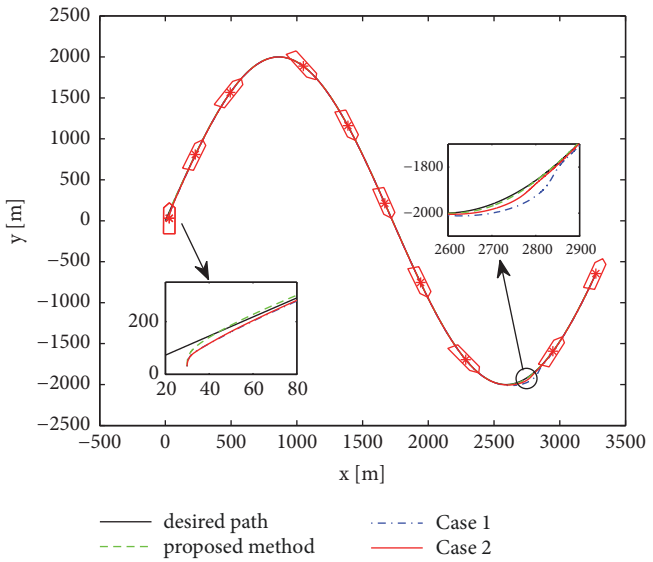

Figure 6: Curvilinear path following.

of the tracking accuracy and convergence rate. Figure 7 shows that the path following error constraints cannot be violated under the proposed controller. Neither the along-track error nor the cross-track error exceeds the position constraints k_s and k_e. However, for the Case 1 method, the position tracking errors transgress the predefined constraints. The position constraint problem is also handled by the Case 2 method, in which the path following errors are also regulated within the prescribed bounds. Figure 8 shows the surge speed tracking results under the different control schemes. We can see that the surge speed smoothly and continuously tracks the desired surge speed u_d under the proposed speed controller. However, the surge speed under Cases 1 and 2 is discontinuous and has a large overshoot.

The yaw rate tracking results under the three controllers are presented in Figure 9. When $t < t_s = 408$ s, the desired surge speed is $u_d = 8$ m/s; thus, the yaw rate constraint is calculated as $k_r = 5$ deg/s and the virtual yaw rate constraint is $k_{\alpha_r} = 4$ deg/s. After t_s, u_d increases to 10 m/s; therefore the yaw rate constraint is calculated as $k_r = 4.5$ deg/s and $k_{\alpha_r} = 3.5$ deg/s. The yaw rate tracking error constraint is set as $k_{r_e} = 1 \text{ deg/s} \leq k_r(t) - k_{\alpha_r}(t)$.

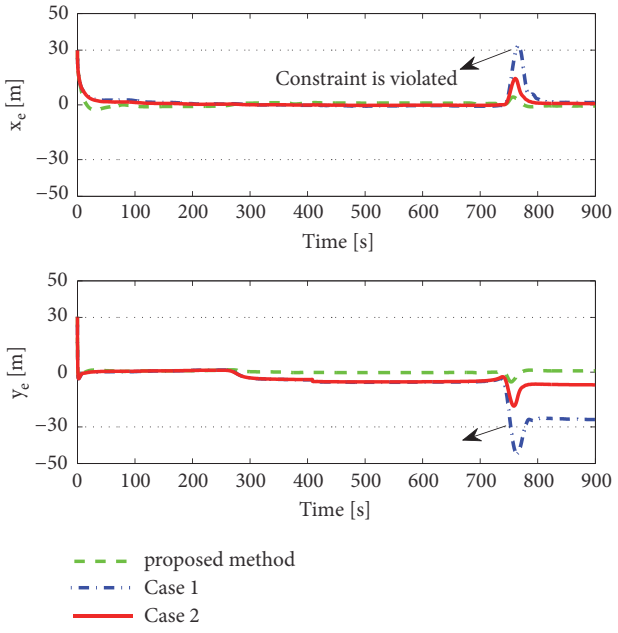

Figure 7: Position errors of curvilinear path following.

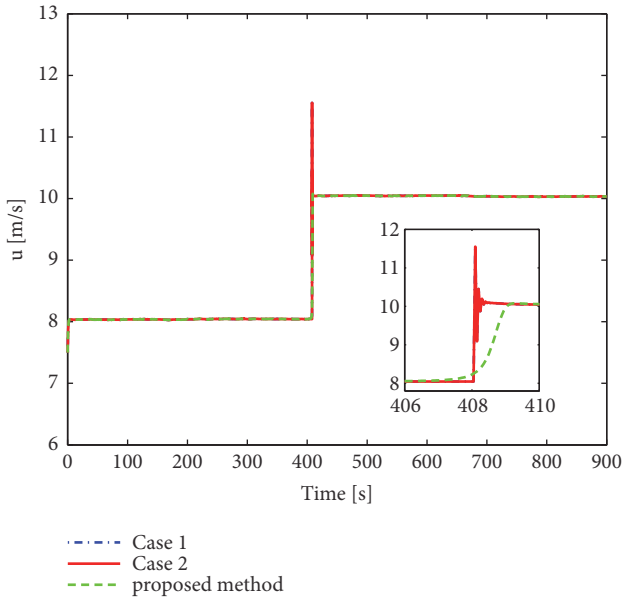

Figure 8: The surge speed of the curvilinear path following.

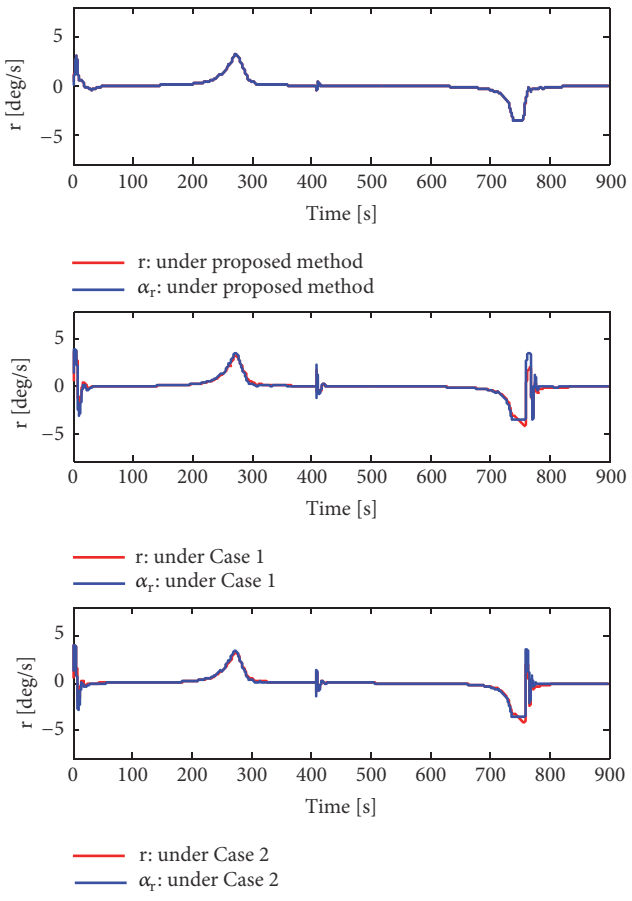

Figure 9: The yaw rate of the curvilinear path following.

In the first subfigure of Figure 9, we observe that the magnitude of the virtual yaw rate $\alpha_r(t)$ is limited by the designed command filter. The yaw rate of the hovercraft has

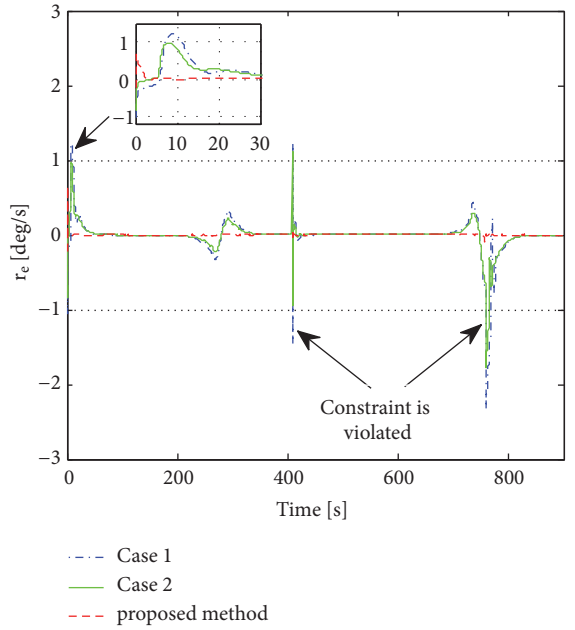

Figure 10: The yaw rate tracking errors of the curvilinear path following.

smaller tracking errors in both transient and steady-state performances, as expected. However, in the second and third figures of Figure 10, it can be observed that the yaw rate tracking errors have large transient and steady-state error. The yaw rate tracking errors under the three controllers are illustrated in Figure 10. The dotted line denotes the yaw rate constraint $k_{r_e}(t)$. It is shown that the yaw rate constraints are guaranteed under the proposed controller, which indicates that the yaw rate of the hovercraft can track the desired yaw rate with the prescribed precision. Therefore, the yaw rate of the hovercraft will never violate the corresponding safety boundary. In contrast, the yaw rate tracking errors under the methods of Cases 1 and 2 both violate the prescribed constraints, because the yaw rate tracking error constraint cannot be guaranteed by using the conventional quadratic Lyapunov function in theory. Due to the page limitation, in Figure 11, the estimate values of the uncertainty parameters in control laws (43) and (55) are shown in the form $\xi_1 = m\widehat{\vartheta}_{u,2}^{\mathrm{T}}\varphi_{u,2}$, $\xi_2 = I_z\widehat{\vartheta}_{r,2}^{\mathrm{T}}\varphi_{r,2}$, $\xi_3 = m\widehat{\vartheta}_{u,1}^{\mathrm{T}}\varphi_{u,1}$, and $\xi_4 = I_z\widehat{\vartheta}_{r,1}^{\mathrm{T}}\varphi_{r,1}$. Figure 12 shows the estimate values $\widehat{D}_u$ and $\widehat{D}_r$. The control inputs τ_u and τ_r are shown in Figure 13; we see that the control signals under our proposed method perform better than another two controllers in terms of oscillations.

5. Conclusion

A constrained adaptive path following control approach has been proposed for a hovercraft under parametric uncertainties and external disturbances. It is shown that the proposed controller can strictly ensure the satisfaction of the prescribed position and velocity constraints by resorting to the barrier Lyapunov function design method. The command filter with a time-varying magnitude limit is employed to generate the

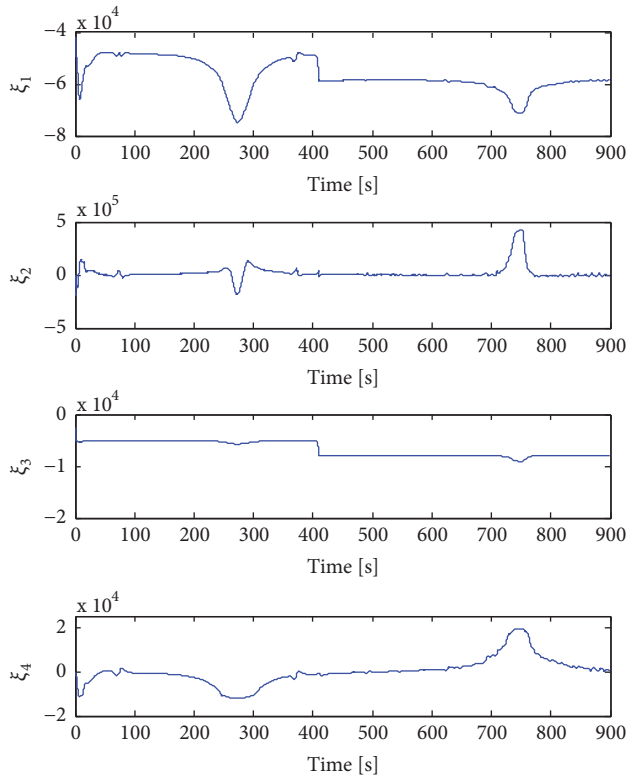

Figure 11: Estimated values of the uncertain parameters.

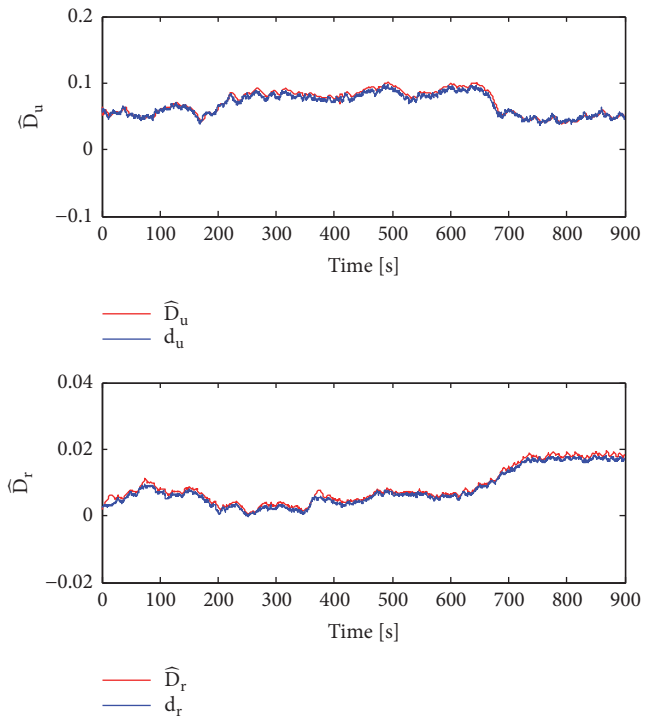

Figure 12: Estimated values of the external disturbances.

desired virtual yaw rate and to reduce the computational complexity, while an auxiliary system is designed to compensate for the estimation error. The uncertain parameters

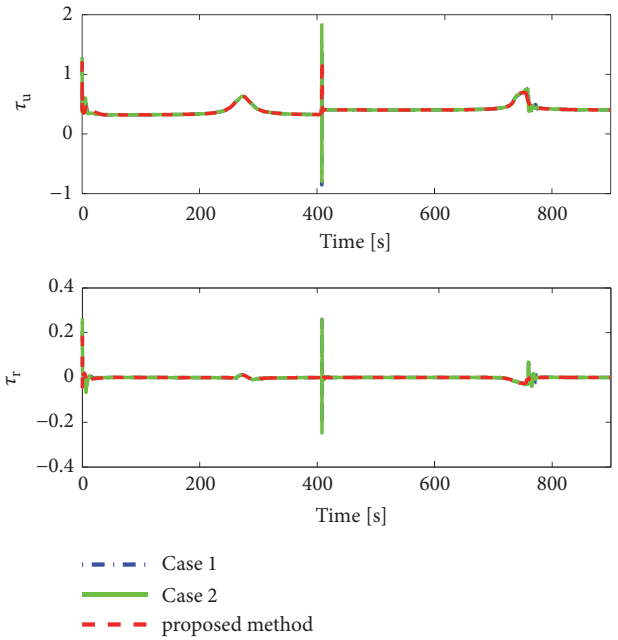

Figure 13: Control inputs of the curvilinear path following.

and the upper bounds of the external disturbances are well estimated by designing parameter adaptation laws. Simulations have indicated the superiority of the proposed control scheme. Because the surge speed of the hovercraft is usually high, the time-varying delay of the measurements may happen. In our future work, we will take into account the time delays in the feedback loop.

Appendix

A. Nominal Values of the Hovercraft Model

The nominal values of the hovercraft are given in Table 1.

B. Expressions of the Hovercraft Model

The expressions of parameters and functions in (7) are given as follows:

$$f_u = -\frac{\rho_a V_a Q \cos\beta}{m},$$

$$f_v = \frac{\left(-\rho_a V_a Q \sin\beta - \rho_a Q_c \left(2p_c/\rho_a\right)^{1/2}\right)}{m},$$

$$f_r = \frac{1}{I_z}\left(-\rho_a V_a Q \sin\beta l_{G_m} - \rho_a Q_c \left(\frac{2p_c}{\rho_a}\right)^{1/2} l_{G_c}\right),$$

$$f_p = \frac{1}{I_x}\left(-\rho_a Q_c \left(\frac{2p_c}{\rho_a}\right)^{1/2} z_g - \rho_a V_a Q \sin\beta \left(z_m - z_g\right) - Wh\tan\phi\right),$$

$$
\begin{aligned}
\vartheta_{u,1} &= S_{xa}\left[C_{xa0}\ \ C_{xa}^{\delta_r}\ \ C_{xa}^{\beta}\ \ C_{xa}^{\dot{\beta}}\right]^{\mathrm{T}},\\
\varphi_{u,1} &= \frac{q_a}{m}\left[1\ \ \delta_r\ \ \beta\ \ \dot{\beta}\right]^{\mathrm{T}},\quad \text{where } q_a = \frac{1}{2}\rho_a V_a^2.\\
\vartheta_{u,2} &= S_h\left[C_{xh}^{0}\ \ C_{xh}^{\phi}\ \ C_{xh}^{\beta}\right]^{\mathrm{T}},\\
\varphi_{u,2} &= \frac{q_h}{m}\left[1\ \ \phi\ \ \beta\right]^{\mathrm{T}},\quad \text{where } q_h = \frac{1}{2}\rho_h U^2.\\
\vartheta_{v,1} &= S_{ya}\left[C_{ya0}\ \ C_{ya}^{\delta_r}\ \ C_{ya}^{\beta}\ \ C_{ya}^{\dot{\beta}}\right]^{\mathrm{T}},\\
\varphi_{v,1} &= \varphi_{u,1},\\
\vartheta_{v,2} &= S_h\left[C_{yh}^{0}\ \ C_{yh}^{\phi}\ \ C_{yh}^{\beta}\right]^{\mathrm{T}},\\
\varphi_{v,2} &= \varphi_{u,2},\\
\vartheta_{r,1} &= S_{za}\left[C_{mza0}\ \ C_{mza}^{\delta_r}\ \ C_{mza}^{\beta}\ \ C_{mza}^{\dot{\beta}}\right]^{\mathrm{T}},\\
\varphi_{r,1} &= \frac{q_a l_a}{I_z}\left[1\ \ \delta_r\ \ \beta\ \ \dot{\beta}\right]^{\mathrm{T}},\\
\vartheta_{r,2} &= S_h\left[C_{mzh}^{\phi}\ \ C_{mzh}^{\beta}\right]^{\mathrm{T}}\\
\varphi_{r,2} &= \frac{q_h l_c}{I_z}\left[\phi\ \ \beta\right]^{\mathrm{T}},\\
\vartheta_{p,1} &= \vartheta_{v,1},\\
\vartheta_{p,2} &= \vartheta_{v,2},\\
\varphi_{p,1} &= \frac{q_a z_a}{I_x}\left[1\ \ \delta_r\ \ \beta\ \ \dot{\beta}\right]^{\mathrm{T}},\\
\varphi_{p,2} &= \frac{q_h z_g}{I_x}\left[\phi\ \ \beta\right]^{\mathrm{T}}.
\end{aligned}
\tag{B.1}
$$

Data Availability

The data in this paper is derived from the International cooperation projects. Hence the date is private.

Conflicts of Interest

The authors declare that there are no conflicts of interest regarding the publication of this paper.

Acknowledgments

This work was supported by the National Natural Science Foundation of China under grant 51309062.

References

[1] L. Yun and A. Bliault, *Theory & Design of Air Cushion Craft*, Butterworth-Heinemann, Oxford, UK, 2000.

[2] J. A. Fein, A. H. Magnuson, and D. D. Moran, "Dynamic performance characteristics of an air cushion vehicle," *Journal of Hydronautics*, vol. 9, no. 1, pp. 13–24, 1975.

[3] R. Hayashi, K. Osuka, and T. Ono, "Trajectory control of an air cushion vehicle," in *Proceedings of the IEEE/RSJ International Conference on Intelligent Robots and Systems '94 (IROS '94), 'Advanced Robotic Systems and the Real World (IROS'94)*, pp. 1906–1913, Munich, Germany, 1994.

[4] M. Breivik and T. I. Fossen, "Path following for marine surface vessels," in *Proceedings of the Ocean'04 - MTS/IEEE Techno-Ocean'04: Bridges across the Oceans - Conference Proceedings*, vol. 4, pp. 2282–2289, Japan, November 2004.

[5] Z. Li, J. Sun, and S. Oh, "Design, analysis and experimental validation of a robust nonlinear path following controller for marine surface vessels," *Automatica*, vol. 45, no. 7, pp. 1649–1658, 2009.

[6] S. Oh and J. Sun, "Path following of underactuated marine surface vessels using line-of-sight based model predictive control," *Ocean Engineering*, vol. 37, no. 2-3, pp. 289–295, 2010.

[7] C. Liu, R. R. Negenborn, X. Chu, and H. Zheng, "Predictive path following based on adaptive line-of-sight for underactuated autonomous surface vessels," *Journal of Marine Science and Technology (Japan)*, vol. 23, no. 3, pp. 483–494, 2018.

[8] T. I. Fossen and A. M. Lekkas, "Direct and indirect adaptive integral line-of-sight path-following controllers for marine craft exposed to ocean currents," *International Journal of Adaptive Control and Signal Processing*, vol. 31, no. 4, pp. 445–463, 2017.

[9] Y.-X. Li and G.-H. Yang, "Model-based adaptive event-triggered control of strict-feedback nonlinear systems," *IEEE Transactions on Neural Networks and Learning Systems*, vol. 29, no. 4, pp. 1033–1045, 2018.

[10] Z. Zheng and L. Sun, "Path following control for marine surface vessel with uncertainties and input saturation," *Neurocomputing*, vol. 177, pp. 158–167, 2016.

[11] L. Liu, D. Wang, and Z. Peng, "Path following of marine surface vehicles with dynamical uncertainty and time-varying ocean disturbances," *Neurocomputing*, vol. 173, pp. 799–808, 2016.

[12] K. Shojaei, "Neural adaptive robust control of underactuated marine surface vehicles with input saturation," *Applied Ocean Research*, vol. 53, pp. 267–278, 2015.

[13] H. Sira-Ramírez and C. A. Ibáñez, "On the control of the hovercraft system," *Dynamics and Control. An International Journal*, vol. 10, no. 2, pp. 151–163, 2000.

[14] A. P. Aguiar, L. Cremean, and J. P. Hespanha, "Position tracking for a nonlinear underactuated hovercraft: Controller design and experimental results," in *Proceedings of the 42nd IEEE Conference on Decision and Control*, pp. 3858–3863, December 2003.

[15] I. Fantoni, R. Lozano, F. Mazenc, and K. Y. Pettersen, "Stabilization of a nonlinear underactuated hovercraft," in *Proceedings of the 38th IEEE Conference on Decision and Control (CDC)*, vol. 3, pp. 2533–2538, December 1999.

[16] H. Sira-Ramírez, "Dynamic second-order sliding mode control of the hovercraft vessel," *IEEE Transactions on Control Systems Technology*, vol. 10, no. 6, pp. 860–865, 2002.

[17] Y. Han and X. Liu, "Higher-order sliding mode control for trajectory tracking of air cushion vehicle," *Optik - International Journal for Light and Electron Optics*, vol. 127, no. 5, pp. 2878–2886, 2016.

[18] J. Tsinias and I. Karafyllis, "ISS property for time-varying systems and application to partial-static feedback stabilization

and asymptotic tracking," *Institute of Electrical and Electronics Engineers Transactions on Automatic Control*, vol. 44, no. 11, pp. 2179–2184, 1999.

[19] S. S. Pavlichkov, S. N. Dashkovskiy, and C. K. Pang, "Uniform stabilization of nonlinear systems with arbitrary switchings and dynamic uncertainties," *Institute of Electrical and Electronics Engineers Transactions on Automatic Control*, vol. 62, no. 5, pp. 2207–2222, 2017.

[20] H. Wu, "Simple adaptive robust output tracking control schemes of uncertain parametric strict-feedback non-linear systems with unknown input saturations," *IET Control Theory & Applications*, vol. 12, no. 12, pp. 1694–1703, 2018.

[21] A. Astolfi, D. Karagiannis, and R. Ortega, *Nonlinear and Adaptive Control with Applications*, Springer, London, UK, 2008.

[22] M. Krstić, I. Kanellakopoulos, and P. Kokotović, "Adaptive nonlinear control without overparametrization," *Systems & Control Letters*, vol. 19, no. 3, pp. 177–185, 1992.

[23] G. Zhang, X. Zhang, and Y. Zheng, "Adaptive neural path-following control for underactuated ships in fields of marine practice," *Ocean Engineering*, vol. 104, pp. 558–567, 2015.

[24] G. Zhang and X. Zhang, "A novel DVS guidance principle and robust adaptive path-following control for underactuated ships using low frequency gain-learning," *ISA Transactions*, vol. 56, pp. 75–85, 2015.

[25] J. Shin, D. J. Kwak, and Y.-I. Lee, "Adaptive path-following control for an unmanned surface vessel using an identified dynamic model," *IEEE/ASME Transactions on Mechatronics*, vol. 22, no. 3, pp. 1143–1153, 2017.

[26] T. I. Fossen and K. Y. Pettersen, "On uniform semiglobal exponential stability (USGES) of proportional line-of-sight guidance laws," *Automatica*, vol. 50, no. 11, pp. 2912–2917, 2014.

[27] K. Y. Pettersen, "Lyapunov sufficient conditions for uniform semiglobal exponential stability," *Automatica*, vol. 78, pp. 97–102, 2017.

[28] A. M. Lekkas and T. I. Fossen, "Integral LOS path following for curved paths based on a monotone cubic hermite spline parametrization," *IEEE Transactions on Control Systems Technology*, vol. 22, no. 6, pp. 2287–2301, 2014.

[29] T. I. Fossen, K. Y. Pettersen, and R. Galeazzi, "Line-of-sight path following for dubins paths with adaptive sideslip compensation of drift forces," *IEEE Transactions on Control Systems Technology*, vol. 23, no. 2, pp. 820–827, 2015.

[30] L. Liu, D. Wang, Z. Peng, and T. Li, "Modular adaptive control for LOS-based cooperative path maneuvering of multiple underactuated autonomous surface vehicles," *IEEE Transactions on Systems, Man, and Cybernetics: Systems*, vol. 47, no. 7, pp. 1613–1624, 2017.

[31] L. Liu, D. Wang, and Z. Peng, "ESO-based line-of-sight guidance law for path following of underactuated marine surface vehicles with exact sideslip compensation," *IEEE Journal of Oceanic Engineering*, vol. 42, no. 2, pp. 477–487, 2017.

[32] J. Miao, S. Wang, M. M. Tomovic, and Z. Zhao, "Compound line-of-sight nonlinear path following control of underactuated marine vehicles exposed to wind, waves, and ocean currents," *Nonlinear Dynamics*, vol. 89, no. 4, pp. 2441–2459, 2017.

[33] R. Gran, G. Carpenter, and R. W. Klein, "Computer aided design of a control system for a hovercraft," in *Proceedings of the 21st IEEE Conference on Decision and Control*, vol. 21, pp. 1347–1353, 1982.

[34] D. Q. Mayne, J. B. Rawlings, C. V. Rao, and P. O. M. Scokaert, "Constrained model predictive control: stability and optimality," *Automatica*, vol. 36, no. 6, pp. 789–814, 2000.

[35] M. Krstic and M. Bement, "Nonovershooting control of strict-feedback nonlinear systems," *IEEE Transactions on Automatic Control*, vol. 51, no. 12, pp. 1938–1943, 2006.

[36] Z. Zheng and M. Feroskhan, "Path following of a surface vessel with prescribed performance in the presence of input saturation and external disturbances," *IEEE/ASME Transactions on Mechatronics*, vol. 22, no. 6, pp. 2564–2575, 2017.

[37] K. P. Tee and S. S. Ge, "Control of nonlinear systems with full state constraint using a barrier lyapunov function," in *Proceedings of the 48th IEEE Conference on Decision and Control Held Jointly with 28th Chinese Control Conference (CDC/CCC '09)*, pp. 8618–8623, Shanghai, China, December 2009.

[38] B. Niu, D. Wang, H. Li, X. Xie, N. D. Alotaibi, and F. E. Alsaadi, "A novel neural-network-based adaptive control scheme for output-constrained stochastic switched nonlinear systems," *IEEE Transactions on Systems, Man, and Cybernetics: Systems*, vol. 49, no. 2, pp. 418–432, 2019.

[39] K. P. Tee, S. S. Ge, and E. H. Tay, "Barrier Lyapunov functions for the control of output-constrained nonlinear systems," *Automatica*, vol. 45, no. 4, pp. 918–927, 2009.

[40] C. Wang, Y. Wu, and J. Yu, "Barrier Lyapunov functions-based dynamic surface control for pure-feedback systems with full state constraints," *IET Control Theory & Applications*, vol. 11, no. 4, pp. 524–530, 2017.

[41] B. Niu and J. Zhao, "Barrier Lyapunov functions for the output tracking control of constrained nonlinear switched systems," *Systems & Control Letters*, vol. 62, no. 10, pp. 963–971, 2013.

[42] H. An, H. Xia, and C. Wang, "Barrier Lyapunov function-based adaptive control for hypersonic flight vehicles," *Nonlinear Dynamics*, vol. 88, no. 3, pp. 1833–1853, 2017.

[43] X. Wang, Y. Zhang, and H. Wu, "Sliding mode control based impact angle control guidance considering the seekers field-of-view constraint," *ISA Transactions*, vol. 61, pp. 49–59, 2015.

[44] X. Jin, "Adaptive fault tolerant control for a class of input and state constrained MIMO nonlinear systems," *International Journal of Robust and Nonlinear Control*, vol. 26, no. 2, pp. 286–302, 2016.

[45] Z. Zheng, L. Sun, and L. Xie, "Error-constrained los path following of a surface vessel with actuator saturation and faults," *IEEE Transactions on Systems, Man, and Cybernetics: Systems*, vol. 48, no. 10, pp. 1794–1805, 2018.

[46] K. P. Tee, B. Ren, and S. S. Ge, "Control of nonlinear systems with time-varying output constraints," *Automatica*, vol. 47, no. 11, pp. 2511–2516, 2011.

[47] M. Chen, S. S. Ge, and B. Ren, "Adaptive tracking control of uncertain MIMO nonlinear systems with input constraints," *Automatica*, vol. 47, no. 3, pp. 452–465, 2011.

[48] T. I. Fossen, *Handbook of Marine Craft Hydrodynamics and Motion Control*, John Wiley & Sons, New York, NY, USA, 2011.

[49] J. A. Farrell, M. Polycarpou, M. Sharma, and W. Dong, "Command filtered backstepping," *IEEE Transactions on Automatic Control*, vol. 54, no. 6, pp. 1391–1395, 2009.

[50] X. Wang, Z. Chen, and Z. Yuan, "Design and analysis for new discrete tracking-differentiators," *Applied Mathematics-A Journal of Chinese Universities Series B*, vol. 18, no. 2, pp. 214–222, 2003.

[51] X. Bu, X. Wu, M. Tian, J. Huang, R. Zhang, and Z. Ma, "High-order tracking differentiator based adaptive neural control of a flexible air-breathing hypersonic vehicle subject to actuators constraints," *ISA Transactions*, vol. 58, pp. 237–247, 2015.

[52] T. I. Fossen, "How to incorporate wind, waves and ocean currents in the marine craft equations of motion," in *Proceedings of the 9th IFAC Conference on Manoeuvring and Control of Marine Craft*, vol. 45, no. 27, pp. 126–131, 2012.